Effect of Mechanochemically Functionalized Multilayer Graphene on the Tribological Properties of Silicon Carbide/Graphene Nanocomposites in Aqueous Environment

Wenli Zhang[a†], Christian Schröder[b†], Bernadette Schlüter[b], Martin Knoch[c], Ján Dusza[d], Richard Sedlák[d], Rolf Mülhaupt[a], Andreas Kailer[b]

[a] Freiburg Materials Research Center (FMF) and Institute for Macromolecular Chemistry of the University of Freiburg, Stefan-Meier-Str. 21, 79104 Freiburg, Germany.
[b] Fraunhofer Institute for Mechanics of Materials IWM, Woehlerstr. 11, 79108 Freiburg, Germany.
[c] FCT Ingenieurkeramik GmbH, Gewerbepark 11, 96528 Frankenblick, Germany.
[d] Institute of Materials Research, Slovak Academy of Sciences, Division of Ceramic and Non-Metallic Systems, Watsonova 47, 040 01 Košice, Slovak Republic.
E-mail: wenli.zhang@fmf.uni-freiburg.de
† *These authors contributed equally to this work.

ABSTRACT: Dry milling of graphite in a ball mill represents a versatile one-step mechanochemical process for fabricating mechanochemically functionalized multilayer graphene (MG) bearing different functional groups. The variation of the milling parameters enables to control particle size, shape, functionality, specific surface area and dispersability of the MG functional fillers. In this study, MG was used as functional nanofiller for the production of SiC/MG nanocomposites. The nanocomposites exhibit significantly improved tribological behavior. The results of rotating pin on disc sliding tests show that with SiC/MG a noticeable improvement of friction and wear behavior under water-lubricated conditions like in slide bearings and face seals can be achieved. Sliding friction systems with the variant SiC+2% MG-CO_2-120h appear to have the most promising tribological properties, due to the reduced size of the homogeneously distributed graphite particles, which promote the formation of advantageous surface states.

Keywords: silicon carbide; graphene; nanocomposite; mechanochemistry; tribology

1. Introduction

Among advanced ceramic materials, silicon carbides (SiC) have proved their superior wear resistance as well as mechanical, thermal and chemical properties in a wide range of industrial applications and energy production [1–3]. Especially in slide bearings and face seals in aqueous media, SiC ceramics are superior to metallic and polymer materials. However, there is a need to improve the reliability, efficiency and lifetime of these systems by developing the materials. Special attention is paid to components that are used under severe conditions and only lubricated by the surrounding media that are mainly aqueous. Mechanical, electrical, thermal and tribological properties are enhanced by optimising the production process, microstructural design or by adding a filler [4–6].

Recently, graphene, a monolayer of sp^2-hybridised carbon atoms arranged in a two-dimensional lattice, has attracted tremendous attention due to exceptional thermal, mechanical, and electrical properties [7]. There are different techniques to produce graphene. Defect-free graphene with exceptional properties, mainly produced by chemical vapor deposition (CVD), is very expensive and the production volumes are still not large enough to use them as fillers in different nanocomposites for technical applications [8, 9].

In recent years, new cost effective high quality functionalized few layered graphene (FG) was developed, which is an alternative to the more expensive defect-free monolayered graphene. Typically, FG was produced at markedly larger scale by the oxidation of graphite and followed by thermal [10–12] or chemical [13, 14] reduction. However, the production of intermediate graphite oxide (GO) required the use of large amounts of strong acids, hazardous oxidizing agents [15] and frequently also toxic reducing agents such as sodium borohydride [14]. Another approach towards FG preparation exploits dry ball milling of graphite under different gas atmospheres, which enables the one-step synthesis of functionalized graphene with multilayered structures bearing different functional groups. Due to the drastically reduced costs, the hereby produced mechanochemically functionalized multilayer graphene (MG) can be easily upscaled [16–18]. The incorporation of functional groups and higher surface area increased interfacial coupling at matrix/FG interfaces and additionally proved the dispersability of graphene in organic solvents and water [19, 20]. In contrast to the number of publications on polymer/graphene [21–23]. and metal/graphene [24] nanocomposites, the research on ceramics/graphene nanocomposites is less intensive, especially SiC/graphene nanocomposites have been subject to little research to date.

Several research works confirmed that incorporation of fine graphene sheets in the ceramic matrix can effectively improve the mechanical, electrical and tribological behavior, which were detailed described in the reviews of Markandan [25], Nieto [26] and Miranzo [27]. Kvetková et al. [28] prepared and characterized silicon nitride based nanocomposites with different amounts of graphene reinforcement. The fracture toughness was significantly improved from 7 to 10 MPa·$m^{1/2}$ with only 1 wt% graphene. Román-Manso [29] and coauthors reported an electrical conductivity of 4380 S/m for SiC nanocomposites

with 20 vol.% graphene, which were prepared by liquid-phase spark plasma sintering (SPS). Moreover, the research of Amann et al. [30] showed that electric potentials have an effect on the friction and wear behavior of SiC ceramics under water-lubricated conditions. Furthermore, the group of Sedlák [31] presented improved fracture toughness of B_4C/graphene nanocomposites which are 20 % higher in comparison to standard B4C. Furthermore, the wear resistance of tribosystems with these modified materials is 60 % higher unlike systems which do not contain graphene. Porwal et al. [32] used graphene to reduce the coefficient of friction of silica ceramics by 20 % and improve the wear resistance by a factor of 8.5 compared to silica nanocomposites. In addition, Miranzo et al. [33] found a 100 % improvement in thermal conductivity of silicon nitride nanocomposites with 16 vol.% graphene. With regard to silicon nitride materials, Balazsi et al. [34] reported improved tribological properties with microstructures containing multilayered graphene (MLG).

To the best of our knowledge, there is only two publications dealing with tribological effects of SiC/graphene nanocomposites, which was tested under dry sliding conditions [35] or lubricated with isooctane [36]. It was observed by Llorente et al. [35, 36], that SiC/graphene nanocomposites have a strong beneficial effect on wear by building an adhered protective tribofilm. The friction was not changed under dry sliding conditons, during the test under issoctane showed decreases on friction up to 30% independently of the applied load. Besides that, the tribological properties of SiC/graphene nanocomposites in aqueous environment, which are close to the real application of composite like in pumps, are still unexplored, especially with cost efficient MG.

In this work, we examine the influence of mechanochemically functionalized multilayer graphene (MG), prepared by ball milling of graphite under argon, carbon dioxide and nitrogen atmosphere, on the mechanical and tribological properties of SiC/graphene nanocomposites. Here, we used only 2 wt% MG as functional filler, as higher graphene content induced more porosity in the ceramic matrix and reduced the mechanical properties, i.e. hardness and elastic modulus [31, 35, 37, 38]. In contrast to the tribological test with dry conditions from Llorente et al. [35] or lubricated with isooctane [36], the friction and wear behavior was tested here in aqueous environment.

2. Experimental

2.1 Synthesis of mechanochemically functionalized multilayer graphene (MG) and its dispersions

Mechanochemically functionalized multilayer graphene (MG) was prepared by milling dried (48 h at 60 °C, 10 mbar) natural graphite (18.6 g, KFL99.5, Graphite Kropfmühl AG, Hauzenberg, Germany) in a planetary ball mill (PM 100, Retsch GmbH, Haan, Germany) The ball mill reactor was made of yttria-stabilized zirconia having a volume of 1150 cm^3 and was equipped with 100 yttria-stabilized zirconia balls (diameter 10 mm, Retsch GmbH, Haan, Germany) using a custom-made stainless steel lid. The milling jar was dried (48 h at 40 °C, 10 mbar) and evacuated (0.1 mbar, 15 min) and pressurized with Ar, CO_2, or N_2, respectively, at 13 bar. Milling was performed at 250 rpm for the duration of 24 h, 48 h, 72 h, 96 h or 120 h in the case of CO_2. For grinding under N_2 or Ar pressure the milling time was 72 h. The milled samples were discharged from the ball mill in air. High purity argon (>99.9 %), carbon dioxide (>99.9 %) and nitrogen (>99.9 %) were obtained from Air Liquide (Paris, France) and used without further purification.

Elemental Analysis (carbon, hydrogen and nitrogen content) was performed by using a vario MICRO cube (Elementar Analysensysteme GmbH, Langenselbold, Germany). The oxygen and zirconium content was determined with energy-dispersive X-ray spectroscopy by using an x-act (Oxford Instruments, Abingdon, United Kingdom) with an accelerating voltage of 20 kVor 30 kV. Fourier transform infrared spectroscopy (FT-IR) was performed with KBr tablets containing the sample. Typically, 32 scans with a resolution of 2 cm^{-1} were recorded on a Vektro 22 (Bruker, Massachusetts, United States). Scanning electron microscopy images were obtained by using a Quanta 250 FEG (FEI, Oregon, United States) with an ETD detector and an accelerating voltage of 20 kV or 30 kV for MG. The specific surface area was performed by adsorption of nitrogen according to Brunauer-Emmett-Teller (BET) theory by using a Sorptomatic 1990 (POROTEC GmbH, Hofheim am Taunus, Germany). Thermal gravimetric analysis (TGA) of produced MG materials was carried out on a STA 409 (NETZSCH GmbH, Selb, Germany). The samples were heated in nitrogen atmosphere from 50 °C to 1500 °C with a heating rate of 10 K/min.

To generate a homogenous distribution of graphene in SiC matrix, the MG nanofillers were prepared as a stable dispersion. MG materials were predispersed in distilled water (10 g/L) for 30 min using an ultrasonic bath Sonorex Super RK 255H (BANDELIN electronic GmbH, Berlin, Germany). Afterwards, the stable MG dispersions were prepared with a high pressure homogenizer Panda NS001 from GEA Niro Soavi (Düsseldorf, Germany) at 1000 bar without using any surfactants or binders.

Stability analysis and average particle size of the MG dispersions at room temperature was determined with an analytical ultracentrifuge LUMiSizer (LUM GmbH, Berlin, Germany). The freshly prepared dispersions (1 g/L) were measured at a rotation speed of 1000 rpm and a temperature of 25 °C for 100,000 s (approx. 28 h) with an interval of 10 s. The measurements were repeated at least three times. Transmission electron microscopy (LEO 912 Omega, Zeiss, Oberkochen, Germany) of graphene samples was performed with an accelerating voltage of 120 kV. The samples were directly collected from dispersions (1 mg/ml, in acetone) on Cu grids.

2.2 Production of SiC/Graphene Nanocomposites

2 wt% ceramic nanocomposite slurries were prepared by blending the already prepared aqueous MG dispersion together with SiC (13 m^2/g, d_{90} = 2 µm) and sintering aid B_4C and carbon black in a planetary ball mill (PM 4, Retsch GmbH, Haan, Germany) for the duration of 4 h and a Sharker Mixer (TURBULA Type T2F, Willy A. Bachofen AG, Basel, Switzerland) for 4 h. After homogenization, the slurries were dried by freeze drying, and large particles were removed by subsequent sieving through a 63 µm mesh. Then, the dried samples were isostatically compressed at 1500 bar. Finally, the samples were sintered at 2050 °C for 4 h under argon atmosphere at ambient pressure.

The density of SiC/graphen nanocomposites was measured by using Archimedes' method in water. The theoretical density of the samples was calculated according to the individual contents of different phases in nanocomposites. The four-point bending strength (σ) values of ceramic nanocomposites were determined by bending tests (7-10 samples) on a tensile/loading machine (LR5K-Plus, Lloyd Instruments, Bognor Road West Sussex, United Kingdom) on the bars with the dimensions 3 mm × 4 mm × 45mm, with inner and outer spans of 20 mm and 40 mm, respectively. They were ground and polished by a D46 wheel before testing. Two edges on the tensile surface were cut to an angle of 45° in order to eliminate a failure initiated from the edge of the specimen. The specimens were broken at a cross-head speed of 0.5 mm/min at ambient temperature and atmosphere. The strength was calculated as the mean value for each composition.

$$\sigma = \frac{3P(S_1 - S_2)}{2BW^2} \quad (1)$$

where P–fracture load, S_1–outer span distance, S_2–inner span distance, B–width of the sample, W–height of the sample.

The fracture toughness was measured by SEVNB method (3-4 samples). The specimens with dimensions 3 mm × 4 mm × 45 mm were ground and polished by a 15 µm diamond grinding wheel before testing. A sharp V-notch using the razor blade and diamond paste (6 µm, 3 µm and 1 µm for the final stage of notching) with total depth between 0.8 mm–1.2 mm was prepared. The specimens were tested in four-point bending fixture on a tensile/loading machine (LR5K-Plus, Lloyd Instruments) with inner and outer spans of 20 mm and 40 mm and crosshead speed of 0.5 mm/min at ambient temperature and atmosphere. In the case of a 4-point flexure, the fracture toughness is then calculated as the mean value for each composition by the following equations:

$$K_{IC} = \sigma\sqrt{\alpha Y} = \frac{F}{B\sqrt{W}} \cdot \frac{S_1 - S_2}{W} \cdot \frac{3\sqrt{\alpha}}{2(1-\alpha)^{1.5}} \cdot Y \quad (2)$$

$$Y = 1.9887 - 1.326\alpha - \frac{(3.49 - 0.68\alpha + 1.35\alpha^2)\alpha(1-\alpha)}{(1+\alpha)^2} \quad (3)$$

$$\alpha = \frac{a}{W} \quad (4)$$

Where K_{IC}–fracture toughness, σ–fracture strength, F–fracture load, B–specimen thickness, W–specimen width, S_1–outer span distance, S_2–inner span distance, a–average V-notch length, α–relative V-notch depth, Y–stress intensity shape factor. To investigate the influence of grinding time on strength and fracture toughness, these mechanical values were measured for samples containing graphene, which was ground at the lowest and highest durations.

2.3. Tribological tests

Sliding tests of graphene-infiltrated SiC ceramics against commercially available SSiC face seal counter ring (Hexoloy SA, Eagle Burgmann Germany, Wolftratshausen, Germany) were performed using a standard pin-on-ring setup (TRM 1000, Dr.-Ing. Georg Wazau Mess- + Prüfsysteme GmbH, Berlin, Germany). The initial graphene-containing pins had a spherical tip with a radius of 5 mm at the front edge and had dimensions of 10 mm x 4 mm x 4 mm in length, width and thickness. The contact geometry of a spherical calotte ensures that an initial point contact is established thus there is no risk of the surfaces tilting. The initial contact stresses can be calculated according to Hertz's equations. The normal force and sliding speed were 50 N and 0.1 m/s, consequently the initial contact pressure amounts up to 2.7 GPa. Tests were conducted under water-lubricated conditions at room temperature for 4 h and repeated two times. As reference system, SiC pins without graphene were tested against SiC rings under the same conditions. The pins' surfaces were investigated subsequently after the tribological tests via digital microscopy and SEM (ZeissSupra 40VP, Carl Zeiss AG, Oberkochen, Germany) to determine the wear volumes and wear mechanisms. In the SEM analyses, a low electron beam energy and an in-lens detector were used to resolve surface changes due to wear with high contrast. For both, reference system and the best tribosystem, one further test was conducted for 20 h. XPS analysis was used to clarify the chemical bonds on the worn surfaces to detect the deposition of graphene.

3. Results and Discussion

3.1 Synthesis and characterization of mechanochemically functionalized multilayer graphene (MG)

Three different of mechanochemically functionalized multilayer graphene MG nanofillers were produced by mechanochemical functionalization of graphite during ball milling under Ar, CO_2 or N_2 atmosphere, respectively, at 13 bar. As reported by Jeon et al. [17], dry milling of graphite under CO_2 pressure produced edge-selective carboxylated multilayer graphene (MG-CO_2). Moreover, dry ball milling of graphite under N_2 pressure enables the fixation of N_2 at the edges of graphene nanoplatelets. Here, the formation of 5- and 6-membered nitrogen containing aromatic rings at the edges of the

graphene was proposed (MG-N_2) [16]. In contrast, dry milling of graphene under argon pressure produced active carbon species and dangling bonds instead of functional groups. After the milling process during the exposure to air these active carbons react with O_2 and moisture to form hydroxyl functional groups (MG-Ar) [21, 39, 40]. These MG were used as fillers in SiC-based nanocomposites in order to examine their effect on tribological, mechanical and morphological properties. The milling time varied between 24 h and 120 h. For grinding under N_2 or Ar pressure the milling time is limited to 72 h because because the yttria-stabilized zirconia balls generate a high Zr abrasion (compare Zr content in Table 1). After milling, the reactor was discharged in air. The influence of the gas atmosphere and milling time on filler properties like elemental composition, functionality, particle size, specific surface area, thermal stability and morphology was investigated. The elemental composition, specific surface area and thermal stability of produced MG materials are listed in Table 1.

As it is apparent from Table 1, the incorporated functional groups in MG are highly dependent on milling time and gas atmosphere. By milling under Ar pressure the oxygen content increases up to 10 wt%, which corresponds predominantly to hydroxyl groups. FT-IR spectroscopy of MG-Ar (Figure 1b) confirmed the presence of O-H vibration bands at 3450 cm^{-1}. The peak at 1635 cm^{-1} represents the C=C stretching vibration. In addition, the product showed C-H stretching vibration bands at 2923 cm^{-1} and 2852 cm^{-1}, which confirmed the reaction of active carbon with moisture from air. Milling in the presence of CO_2 leads to an increased oxygen content of up to 12 wt%, mainly resulting from the formation of carboxyl groups. The MG-CO_2 (Figure 1c) showed C=O stretching vibration bands at 1733 cm^{-1}, CO_2^- asymmetric stretching at 1578 cm^{-1} and C-O vibration at 1384 cm^{-1}, which typically correspond to carboxyl groups. Dry Milling of graphite in N_2 gives a mechanochemical nitrogen fixation of up to 10 wt%. The absorption bands of MG-N_2 (Figure 1d) at 1630 cm^{-1} originate from C-N or N-H vibrations. In addition, the thermal stability depends on the amount of functional groups. By heating, these functional groups could be removed. For this reason, higher oxygen contents were paralleled higher weight loss in thermal gravimetric measurements (TGA).

Dry milling of graphite leads not only to high functionality, but also to a drastic decrease of aspect ratio and particle size as well as an increase of specific surface area of up to 575 m^2/g (see Table 1). Scanning (SEM) and transmission electron microscopy (TEM) were employed to analyze the particle morphology of the MG materials. SEM images of natural graphite (Figure 2a and b) show the typical platelet-structure with particle sizes of ~300 µm and thickness of 1.6 µm. After 48 h milling under Ar (Figure 2c and d) or N_2 (Figure 2g and h) pressure, respectively, only cubic and spherical nanoparticles with an average diameter (see average particle size in Table 1) of a few nanometers were observed while the typical sheet like structure of natural graphite was absent. In contrast, for MG-CO_2 (Figure 2e and f), in addition to spherical nanoparticles, large and thin platelets were observed.

One of the key problems in graphene applications is the poor dispersability of graphene, which requires the use of surfactants or binders for the production of stable graphene dispersions with high graphene content. This makes the dispersions expensive and impure. In this study, stable MG dispersions with high solids concentration were prepared with a high pressure homogenizer (Panda NS001) at 1000 bar without requiring any surfactants or binders. The stability and instability index of the MG dispersions were measured by using an analytical centrifuge (LUMiSizer). A high instability index corresponds to poor stability of the dispersion. For longer milling time until 96 h of MG-CO_2 an increasing stability of its dispersions was observed (Figure 3). Longer milling times lead to a higher amount of incorporated hydrophilic groups, which enhances the stability of the dispersions in water. The stability of the MG-CO_2-120h dispersion decreased in comparison with MG-CO_2-96h, because of the reagglomeration of the little spherical MG particles. As can be seen from the instability index analysis in Figure 3, after the HPH-process the MG dispersions show much lower instability indices and therefore are more stable. Due to the high pressure and high shear forces in this process, the agglomerations in MG dispersions were depleted, thus improving MG dispersion stability by preventing sedimentation of large particles.

Table 1. Production conditions, elemental compositions and physical properties of MG materials.

Sample	Gas	Milling Time [h]	C[(a)] [wt%]	H[(a)] [wt%]	N[(a)] [wt%]	O[(b)] [wt%]	Zr[(b)] [wt%]	Surface area[(c)] [m²/g]	Mass loss TGA[(d)] [wt%]	Particle size(e) [nm]
Graphite	Air	0	99.6	0.2	0.2	0.7	-	3	2.5	~300000
MG-Ar-24h	Ar	24	89.1	0.6	0.6	6.9	0.6	444	9.6	132
MG-Ar-48h	Ar	48	85.7	0.7	0.5	8.4	2.2	351	13.3	134
MG-Ar-72h	Ar	72	81.7	0.6	0.6	9.3	3.8	275	17.3	232
MG-CO_2-24h	CO_2	24	91.5	0.7	-	8.0	-	283	6.4	186
MG- CO_2-48h	CO_2	48	88.2	0.8	-	10.4	-	416	10.9	185
MG- CO_2-72h	CO_2	72	86.4	0.9	-	11.7	-	539	13.7	145
MG- CO_2-96h	CO_2	96	87.9	0.5	-	10.9	-	561	20.7	144
MG- CO_2-120h	CO_2	120	86.4	0.6	-	11.1	0.5	575	28.0	134
MG-N_2-24h	N_2	24	82.2	1.0	4.0	8.4	-	449	20.0	131
MG- N_2-48h	N_2	48	80.2	0.8	6.1	9.0	1.9	269	24.5	118
MG- N_2-72h	N_2	72	75.2	1.1	7.2	7.6	4.5	219	29.3	143

[(a)]Determined by elemental analysis. [(b)]Determined by EDX. [(c)]Determined by BET measurements. [(d)]N_2, 50 °C-1500 °C, 10 K/min. [(e)]Determined with LUMiSizer.

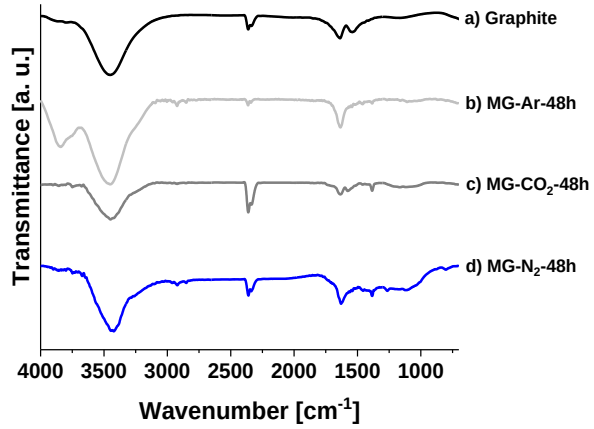

Figure 1. FT-IR spectra of a) Graphite, b) MG-Ar-48h, c) MG-CO_2-48h, d) MG-N_2-48h.

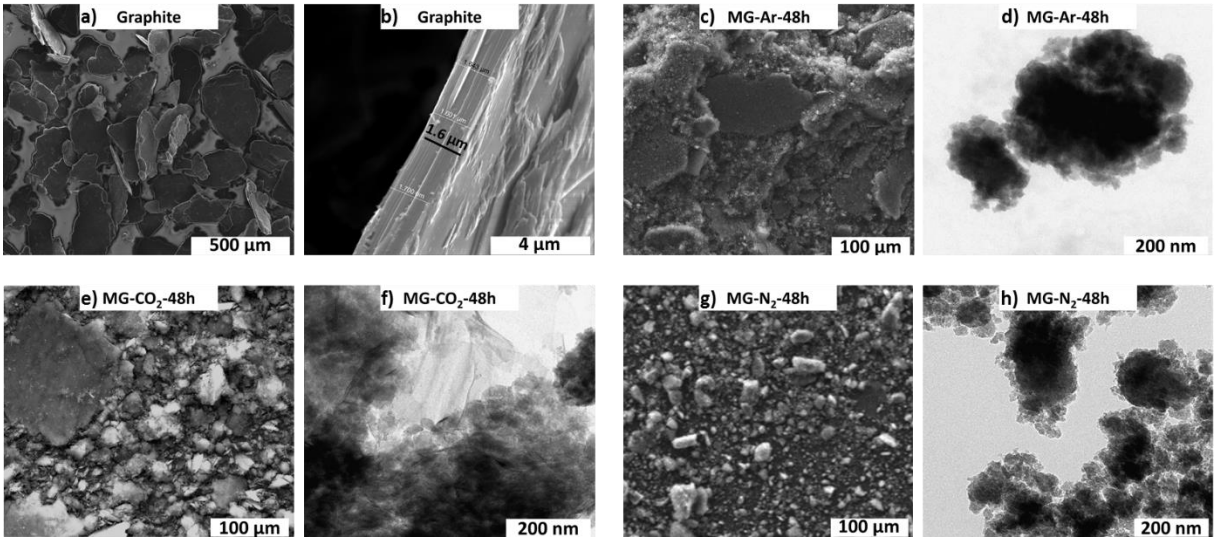

Figure 2. Influence of gas atmosphere on morphology of MG materials. Images of: a, b) graphite (SEM), c) MG-Ar-48h (SEM), d) MG-Ar-48h (TEM), e) MG-CO_2-48h (SEM), f) MG-CO_2-48h (TEM), g) MG-N_2-48h (SEM), h) MG-N_2-48h (TEM).

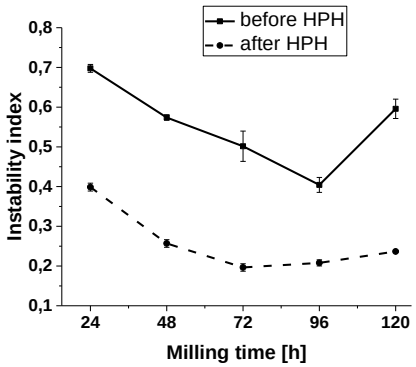

Figure 3. Instability index of MG-CO_2 dispersions in Water (1 g/L) as a function of milling time. The dispersions were produced by sonication (solid line) and high pressure homogenization (HPH) (dashed line).

3.2 Manufactory and Characterization of SiC/graphene Nanocomposites

The MG materials were used as functional fillers for preparing SiC/graphene nanocomposites. The influences of filler type on density, mechanical and tribological properties of nanocomposites were studied.

3.2.1 Density and mechanical properties

The relative density and mechanical properties of investigated SiC/graphene nanocomposites are presented in Table 2. All samples show very high density. It was found that longer milling time of MG-Ar and MG-CO_2 by trend led to higher density. Longer milling time led to more incorporated functional groups, which can enhance the stability of graphene dispersions and increase compatibility of graphene in ceramic matrices. The lowest relative density of 97.7 % was measured for nanocomposites containing 2 wt% MG-CO_2-24h, due to short milling time and low degree of functionalization. This effect of functionality of graphene is exemplarily reflected by the SEM-images of the polished surface of the nanocomposites with different fillers in Figure 4. From the comparison of the microstructures, it can be seen that the amount of big graphene agglomerations in the samples gradually decreased with increasing milling time of MG-CO_2. Furthermore, the distribution of the graphene particles is more homogeneous after long milling durations.

The mechanical properties were determined by flexural measurements. All MG type fillers showed a deterioration of bending strength in comparison to the reference sample. For nanocomposites containing 2 wt% graphene the 4-point bending strength was reduced to values as low as 219 MPa in the case of MG-Ar-24h. Clearly, 4-point bending strength correlated with porosity. In fact, the lower 4 point bending strength of SiC/graphene nanocomposites is attributed to microstructural properties which are generated after the sintering. Here, the complex interactions between residual porosity, MG dispersion and agglomeration may affect the mechanical behaviour. This thesis was confirmed by SEM images of the fracture surfaces of the specimens after 4-point bending strength test. In the nanocomposite with MG-CO_2-48h (Figure 5 c), layer agglomerates were found, while in MG-Ar-48h (Figure 5 b) defects filled with spherical aggregated particles were found. Furthermore, in MG-Ar-48h (Figure 5 b) a crack with a length of more than 50 µm was identified, which is due to an uneven filler distribution and the formation of agglomerates. Despite the high shear forces in the high-pressure homogenizer process, it is not possible to break up all graphene agglomerates. These defects led to a drastic reduction of the maximum loads on the materials and the bending strength. On the other hand, most of the nanocomposites showed similar values of fracture toughness in accordance with the values of the reference material and samples reported in the literature [41, 42]. However, compared to SiC+2% graphite, an improvement in mechanical properties, especially strength, can be observed with SiC/MG. This is due to the high functionality, high specific surface area and good dispersability of MG, which improved interfacial coupling at MG/SiC interfaces and led to homogeneous distribution of MG in SiC matrices.

Table 2. Relative Densities and mechanical properties of SiC/graphene nanocomposites.

Samples	Theoretical density [g/cm^3]	Experimental density [g/cm^3]	Relative density [%]	4-point bending strength [MPa]	SEVNB[a)] fracture toughness [MPa·m$^{1/2}$]
SiC (reference material)	3.174	3.170	99.9	505 ± 65	3.09 ± 0.19
SiC + 2 % Graphite	3.149	3.070	97.5	127 ± 9	2.25 ± 0.35
SiC + 2 % MG-Ar-24h	3.149	3.137	99.6	219 ± 42	3.46 ± 0.17
SiC + 2 % MG-Ar-48h	3.149	3.147	99.9	n/a	n/a
SiC + 2 % MG-Ar-72h	3.149	3.148	100.0	276 ± 28	2.47 ± 0.23
SiC + 2 % MG-CO_2-24h	3.149	3.076	97.7	283 ± 24	2.46 ± 0.11
SiC + 2 % MG-CO_2-48h	3.149	3.106	98.6	n/a	n/a
SiC + 2 % MG-CO_2-72h	3.149	3.114	98.9	n/a	n/a
SiC + 2 % MG-CO_2-96h	3.149	3.106	98.6	n/a	n/a
SiC + 2 % MG-CO_2-120h	3.149	3.132	99.4	283 ± 34	3.02 ± 0.27
SiC + 2 % MG-N_2-24h	3.149	3.142	99.8	325 ± 24	2.80 ± 0.45
SiC + 2 % MG-N_2-48h	3.149	3.142	99.8	n/a	n/a
SiC + 2 % MG-N_2-72h	3.149	3.143	99.8	295 ± 27	3.83 ± 0.89

[a)] Fracture toughness was measured by the Single Edge V-Notched Beam (SEVNB) method.

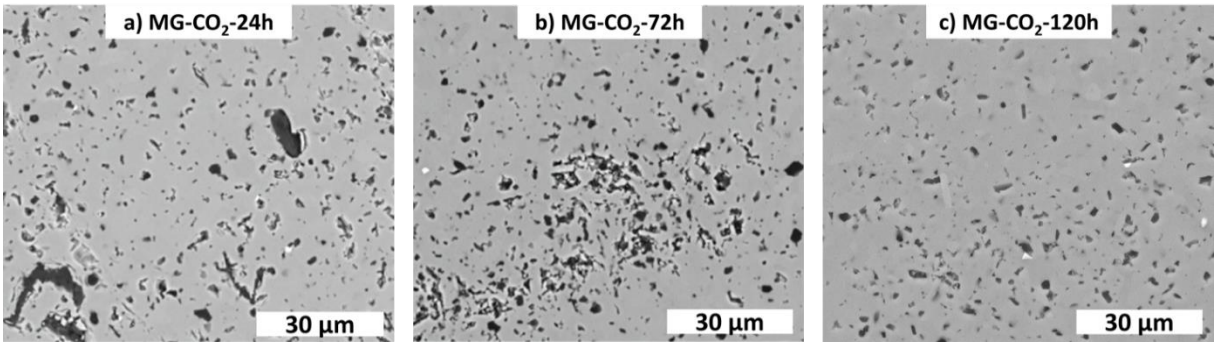

Figure 4: SEM images of SiC microstructures with a): 2 % MG-CO_2-24h, b) 2 % MG-CO_2-72h und c) 2 % MG-CO_2-120h.

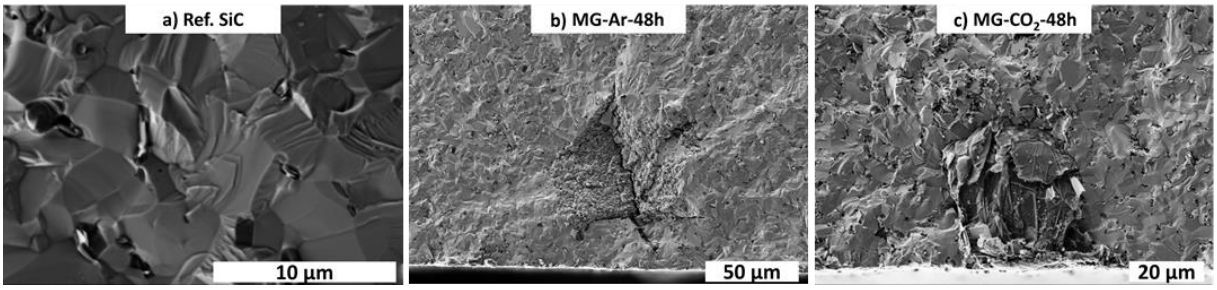

Figure 5: SEM images on fracture surfaces of the sintered (a) reference SiC and SiC nanocomposite with a) 2 % MG-Ar-48h and b) MG-CO_2-48h after the 4-point bending tests.

3.2.2 Tribological properties

Figure 6 (a) displays the friction behavior of different tribosystems using SiC/graphene nanocomposite pins, in which MG was prepared by milling graphite in a CO_2 atmosphere, sliding against SiC rings. For comparison, the black curve depicts development of the reference systems (SiC pins sliding against SiC rings). All tests were carried out 3 times and are well reproducible. The graphs show the average coefficient of friction.

While all tribosystems are characterized by a friction decrease with test duration, the systems based on SiC/MG nanocomposites pins have lower friction in comparison to the reference system comprising SiC sliding against SiC. Furthermore, the different friction curves can be correlated with the MG milling times used for the production of the graphene filler. Longer MG milling times resulted in lower coefficients of friction (COFs). Accordingly, the lowest COFs were in the range of ca. 0.13 for the material containing 2 % MG-CO_2-96 h and 2 % MG-CO_2-120 h, whereas the COF of the reference materials ended with a COF of 0.2. Figure 6 (b) shows the friction behavior of SiC pins containing MG, prepared by milling in N_2 atmosphere and sliding against SiC rings. Again, friction of these tribosystems continuously decreased to values that were significantly lower than the COF of the reference system. Also, the higher milling times during MG production resulted in lower friction of the respective tribosystems, thus COFs in the range of ca. 0.13 were reached. Finally, Figure 6

(c) illustrates the friction behaviors of pins containing MG prepared by milling in Ar atmosphere. In accordance to the friction behavior of the other systems with graphene-containing SiCs, the COFs were still lower than the values of the reference systems. However, the longer milling time to produce the graphene was related to higher friction of the graphene-ceramic nanocomposite. The wear results of the pins are shown in Figure 7.

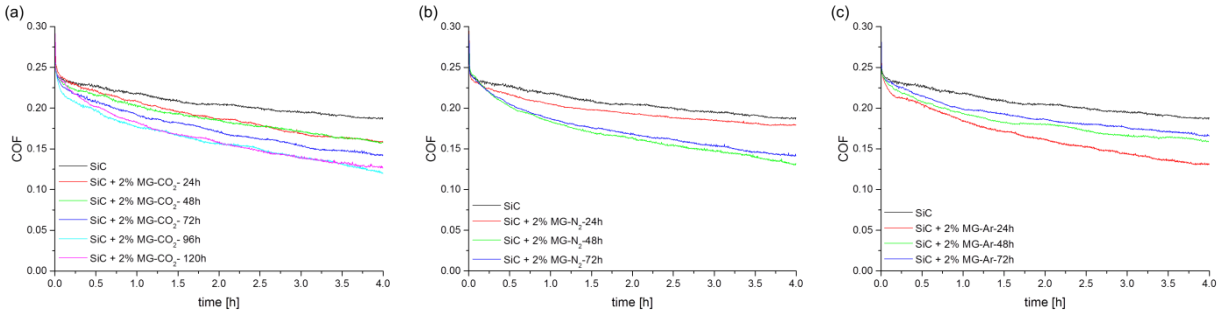

Figure 6: Friction behaviors of different SiC/MG nanocomposite pins sliding against SiC rings for 4 h. (a): MG prepared by milling in CO_2 atmosphere; (b): MG prepared by milling in N_2 atmosphere; (c): MG prepared b milling in Ar atmosphere

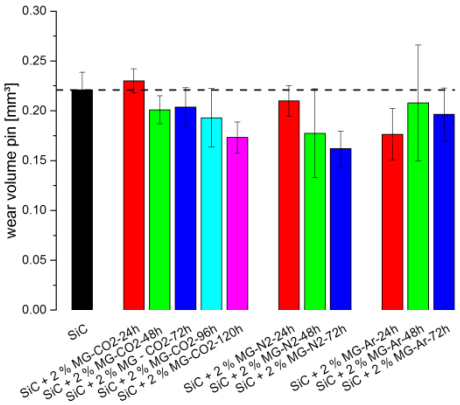

Figure 7: Generated wear of the different graphene-containing SiC/MG nanocomposite pins after sliding against SiC rings for 4 h.

Only the wear of the SiC/MG nanocomposite containing 2 % MG-CO_2-24h was higher with respect to the reference SiC material. For the materials containing MG milled under CO_2 and N_2 atmosphere, a correlation between milling time and wear was derived: Here, higher milling time resulted in decreased wear volumes. Though, this relation is not applicable for SiC/MG nanocomposite pins containing MG produced under Ar atmosphere. According to the friction and wear results, the best material was SiC containing 2 % MG-CO_2-120 h.

Typical results of extended sliding tests are shown in Figure 8.

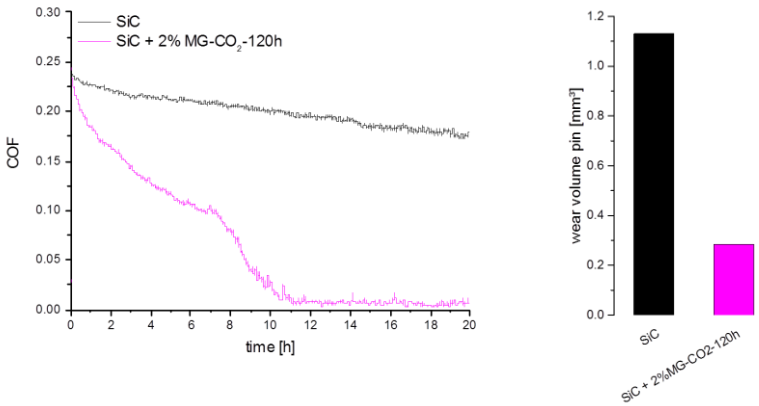

Figure 8: Friction of SiC + 2% MG-CO_2-120h sliding against SiC rings and the reference system (left), the corresponding wear volumes of the pins after a testing duration of 20 h (right).

In agreement with the results presented in Figure 6, the friction of the SiC/MG nanocomposite containing 2 % MG-CO_2-120h is characterized by a continuous decrease with the test duration. All tests were carried out 2 times and are well reproducible. The graphs show the average coefficient of friction. After 7 h and a COF of ca. 0.1, the decrease of the friction curve was even stronger, thus after 11 hours the COF was < 0.01, which was close to the resolution capacity of the tribometer. This value was constant for the rest of the testing time. In contrast, the SiC reference material had a COF in the range of ca. 0.16 after 20 h of testing, even though friction continuously decreased also in this case. The wear of the SiC/MG nanocomposite pin containing 2 % MG-CO_2-120h was essentially lower than the wear of the SiC pin. Setting the wear of both pin materials in relation, the wear volume of the pin made from SiC + 2 % MG-CO_2-120h amounted to 78 % of the wear of the SiC pin after 4 h but only 25 % after 20 h, which is certainly a consequence of the ultralow friction values that were reached after 11 hours.

Fig 8 shows surfaces of SiC pins and SiC pins containing 2 % MG-CO_2-120h.

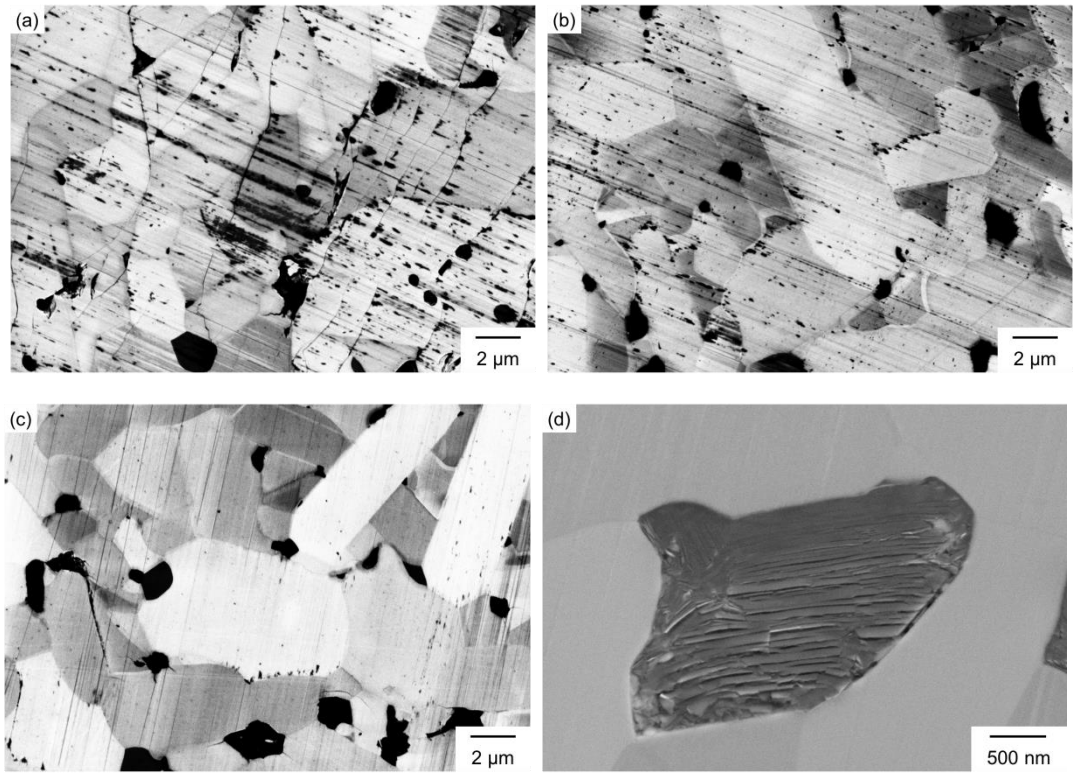

Figure 9: Microscopic images (SEM) of pin surfaces after tribological testing at different loading durations. (a): SiC after 4 h, (b): SiC + 2 % MG-CO_2-120 h after 4 h, (c) + (d): SiC + 2 % MG-CO_2-120 h after 20 h

Grooves running in sliding direction were well visible on the surfaces of both material grades. Furthermore, debris particles which adhered on the surface were visible in different intensities after testing for 4 h and 20 h. In contrast to the surface of SiC + 2 % MG-CO_2-120 h, the surface of the SiC pin was furthermore characterized by local transgranular micro-cracking. The close-up view of the pin surface in Figure 9 (d) shows a layer-by-layer structure of the carbon-containing phase.

These investigations complement the results of previous works [35]. The integration of graphene into the SiC microstructure decreases the wear of the SiC-graphene nanocomposites not only under dry but also under water-lubricated conditions. In contrast to Llorente et al. [35], these SiC/MG nanocomposites result in an essential friction decrease compared to a standard SiC reference material. It is thus assumed that a partial covering of the surface with graphene may protect the surface from mechanical and chemical wear and promotes local hydrodynamic lift. This enables a gradual transition from mixed lubrication conditions to hydrodynamic lubrication, which may be reached after a certain test duration (s. Figure 8) and which corresponds to a threshold contact pressure: Assuming no further wear of the pin with SiC + 2 % MG-CO_2-120h after 7 h, the stresses amount to only 12 MPa from initial maximum Hertzian pressures of ca. 2.7 GPa. This pressure reduction in combination with the development of advantageous surface states (i.e. formation of tribolayers and smoothening of the surfaces) may result in hydrodynamic lubrication.The formation of a stable layer is hard to determine with SEM as tribo-chemical debris can be found on all surfaces even for SiC. But the XPS analysis proves that a nm thick graphene layer was formed on the worn surface of the pin with SiC + 2 % MG-CO_2-120h. In return, the friction reduction positively affects further wear generation, as under less severe mixed lubrication conditions the severity of solid-solid contacts strongly decreases. In contrast, the high COF values for the reference system with SiC indicate that, under

these tribological loading conditions, the surface and geometrical changes do not lead to pronounced lubricating effects, but continuous wear.

With regard to friction, a clear correlation arises between the MG milling duration and the tribological behavior as increasing MG milling time decreases the friction for systems comprising SiC + 2 % MG-CO_2 and 2 % MG-N_2. The increased milling time downsizes the platelet-like graphene particles, which are homogeneously distributed within the SiC microstructure. This promotes the generation of advantageous, graphene-containing surface states which result in low friction and wear. In contrast, for the tribosystems comprising SiC + 2 % MG-Ar the increased friction with increased milling time is the consequence of the spherical morphology and reagglomeration of the corresponding MG particles obtained by prolonged milling. Thus, these microstructures contain of inhomogeneously shaped and distributed graphite particles which are potential flaws and accelerate the wear generation.

4. Conclusions

Mechanochemically functionalized graphene (MG), prepared by milling graphite under various gas atmospheres, represents a promising functional filler for silicon carbide ceramics. Typically, dry milling process in a planetary ball mill under argon, carbon dioxide and nitrogen pressure affords MG as few-layer graphene bearing hydroxyl, carboxyl and nitrogen-functional groups. The variation of the milling parameters (time and gas atmosphere) enables control of particle size, shape, functionality, specific surface area and dispersability of the resulting MG fillers. The incorporation of functional groups and increasing surface area during dry grinding improves interfacial coupling at MG/SiC interfaces and additionally ensures homogenous distribution of MG within the SiC matrix. In contrast to other tedious and rather expensive methods for graphene syntheses, this mechaochemical MG fabrication represents an industrially viable process, which is much more cost and time-efficient, free of solvents and waste. Moreover, stable and dispersant-free MG dispersions can be produced using a high pressure homogenizer and also microfluidizer without adding surfactants. This is highly advantageous with respect to the commercialization of graphene nanofillers for use in the ceramics and plastics industry.

MG-containing SiC microstructures hold great promise with respect to tribological applications under water-lubricated conditions. Several SiC/MG nanocomposite tribosystems with these microstructures afford significantly lower friction and wear as compared to state-of-the-art SiC materials. The MG milling times have a great effect on the tribological properties. Under CO_2 and N_2 atmosphere increasing the duration of the milling process downsizes the platelet-like graphite particles. This again is a necessary condition to produce microstructures with very small and well-distributed MG inclusions which beneficially affect the friction and wear behavior. In contrast, using Ar as inert gas for the milling process, much smaller spherical graphite particles are produced which may agglomerate at prolonged milling times. Thus tribological loading of SiC microstructures with this MG type leads to increased friction and wear. From the tested microstructures it appears that the best tribological properties can be achieved with SiC + 2 % MG-CO_2-120h as pin material under the specified loading conditions. The friction behavior is characterized by a strong decrease of the COF thus indicating the formation of a separation film between the contact partners. The conformal contact promotes a stable water film between the surfaces which is furthermore supported by the formation of a carbon-containing surface layer.

Acknowledgements: The authors gratefully acknowledge the financial support from project ERA.NET-GRACE which is funded by the Federal Ministry of Education and Research (BMBF) under the funding code 03X0156.

References

1. Roewer, G., Herzog, U., Trommer, K., Müller, E., Frühauf, S.: Silicon Carbide — A Survey of Synthetic Approaches, Properties and Applications. In: High Performance Non-Oxide Ceramics I. Springer Berlin Heidelberg, Berlin, Heidelberg (2002)
2. Schwetz, K.A.: Silicon Carbide Based Hard Materials. In: Handbook of Ceramic Hard Materials. Wiley-VCH Verlag GmbH (2008)
3. Friedrichs, P. (ed.): Silicon carbide. Wiley-VCH, Weinheim (2010)
4. Porwal, H., Grasso, S., Reece, M.J.: Review of graphene–ceramic matrix composites. Adv. Appl. Ceram. **8**, 443–454 (2013)
5. Ciudad, E., Sánchez-González, E., Borrero-López, O., Guiberteau, F., Nygren, M., Ortiz, A.L.: Sliding-wear resistance of ultrafine-grained SiC densified by spark plasma sintering with 3Y2O3 + 5Al2O3 or Y3Al5O12 additives. Scr. Mater. **8**, 598–601 (2013)
6. Borrero-López, O., Ortiz, A.L., Guiberteau, F., Padture, N.P.: Microstructural design of sliding-wear-resistant liquid-phase-sintered SiC: An overview. J. Eur. Ceram. Soc. **11**, 3351–3357 (2007)
7. Geim, A.K., Novoselov, K.S.: The rise of graphene. Nat. Mater. **3**, 183–191 (2007)
8. Gomez De Arco, L., Zhang, Y., Schlenker, C.W., Ryu, K., Thompson, M.E., Zhou, C.: Continuous, Highly Flexible, and Transparent Graphene Films by Chemical Vapor Deposition for Organic Photovoltaics. ACS Nano **5**, 2865–2873 (2010)
9. Wang, X., You, H., Liu, F., Li, M., Wan, L., Li, S., Li, Q., Xu, Y., Tian, R., Yu, Z., Xiang, D., Cheng, J.: Large-Scale Synthesis of Few-Layered Graphene using CVD. Chem. Vap. Deposition **1-3**, 53–56 (2009)

10. Tölle, F.J., Fabritius, M., Mülhaupt, R.: Emulsifier-Free Graphene Dispersions with High Graphene Content for Printed Electronics and Freestanding Graphene Films. Adv. Funct. Mater. **6**, 1136–1144 (2012)
11. Aguilar-Bolados, H., Lopez-Manchado, M.A., Brasero, J., Avilés, F., Yazdani-Pedram, M.: Effect of the morphology of thermally reduced graphite oxide on the mechanical and electrical properties of natural rubber nanocomposites. Composites Part B, 350–356 (2016)
12. Zhan, D., Ni, Z., Chen, W., Sun, L., Luo, Z., Lai, L., Yu, T., Wee, A.T.S., Shen, Z.: Electronic structure of graphite oxide and thermally reduced graphite oxide. Carbon **4**, 1362–1366 (2011)
13. Mauro, M., Cipolletti, V., Galimberti, M., Longo, P., Guerra, G.: Chemically Reduced Graphite Oxide with Improved Shape Anisotropy. J. Phys. Chem. C **46**, 24809–24813 (2012)
14. Wei, G., Yu, J., Gu, M., Ai, X., Xu, X., Tang, T.B.: Dielectric relaxation characteristics of chemically reduced graphite oxide. Carbon, 374–379 (2015)
15. Hummers, W.S., Offeman, R.E.: Preparation of Graphitic Oxide. J. Am. Chem. Soc. **6**, 1339 (1958)
16. Jeon, I.-Y., Choi, H.-J., Ju, M.J., Choi, I.T., Lim, K., Ko, J., Kim, H.K., Kim, J.C., Lee, J.-J., Shin, D., Jung, S.-M., Seo, J.-M., Kim, M.-J., Park, N., Dai, L., Baek, J.-B.: Direct nitrogen fixation at the edges of graphene nanoplatelets as efficient electrocatalysts for energy conversion. Sci. Rep., 2260 (2013)
17. Jeon, I.-Y., Shin, Y.-R., Sohn, G.-J., Choi, H.-J., Bae, S.-Y., Mahmood, J., Jung, S.-M., Seo, J.-M., Kim, M.-J., Wook Chang, D., Dai, L., Baek, J.-B.: Edge-carboxylated graphene nanosheets via ball milling. PNAS **15**, 5588–5593 (2012)
18. Jeon, I.-Y., Choi, H.-J., Jung, S.-M., Seo, J.-M., Kim, M.-J., Dai, L., Baek, J.-B.: Large-Scale Production of Edge-Selectively Functionalized Graphene Nanoplatelets via Ball Milling and Their Use as Metal-Free Electrocatalysts for Oxygen Reduction Reaction. J. Am. Chem. Soc. **4**, 1386–1393 (2013)
19. Tölle, F.J., Fabritius, M., Mülhaupt, R.: Emulsifier-Free Graphene Dispersions with High Graphene Content for Printed Electronics and Freestanding Graphene Films. Adv. Funct. Mater. **6**, 1136–1144 (2012)
20. Appel, A.-K., Thomann, R., Mülhaupt, R.: Polyurethane nanocomposites prepared from solvent-free stable dispersions of functionalized graphene nanosheets in polyols. Polymer **22**, 4931–4939 (2012)
21. Beckert, F., Bodendorfer, S., Zhang, W., Thomann, R., Mülhaupt, R.: Mechanochemical Route to Graphene-Supported Iron Catalysts for Olefin Polymerization and in Situ Formation of Carbon/Polyolefin Nanocomposites. Macromolecules **20**, 7036–7042 (2014)
22. Steurer, P., Wissert, R., Thomann, R., Mülhaupt, R.: Functionalized Graphenes and Thermoplastic Nanocomposites Based upon Expanded Graphite Oxide. Macromol. Rapid Commun. **4-5**, 316–327 (2009)
23. Stankovich, S., Dikin, D.A., Dommett, G.H.B., Kohlhaas, K.M., Zimney, E.J., Stach, E.A., Piner, R.D., Nguyen, S.T., Ruoff, R.S.: Graphene-based composite materials. Nature **7100**, 282–286 (2006)
24. Huang, X., Qi, X., Boey, F., Zhang, H.: Graphene-based composites. Chem. Soc. Rev. **2**, 666–686 (2012)
25. Markandan, K., Chin, J.K., Tan, M.T.: Recent progress in graphene based ceramic composites: a review. Journal of Materials Research **1**, 84–106 (2017)
26. Nieto, A., Bisht, A., Lahiri, D., Zhang, C., Agarwal, A.: Graphene reinforced metal and ceramic matrix composites: a review. International Materials Reviews **5**, 241–302 (2017)
27. Miranzo, P., Belmonte, M., Osendi, M. Isabel: From bulk to cellular structures: A review on ceramic/graphene filler composites. J. Eur. Ceram. Soc. **12**, 3649–3672 (2017)
28. Kvetková, L., Duszová, A., Hvizdoš, P., Dusza, J., Kun, P., Balázsi, C.: Fracture toughness and toughening mechanisms in graphene platelet reinforced Si3N4 composites. Scr. Mater. **10**, 793–796 (2012)
29. Román-Manso, B., Domingues, E., Figueiredo, F.M., Belmonte, M., Miranzo, P.: Enhanced electrical conductivity of silicon carbide ceramics by addition of graphene nanoplatelets. J. Eur. Ceram. Soc. **10**, 2723 (2015)
30. Amann, T., Kailer, A., Herrmann, M.: Influence of Electrochemical Potentials on the Tribological Behavior of Silicon Carbide and Diamond-Coated Silicon Carbide. Journal of Bio- and Tribo-Corrosion **4**, 30 (2015)
31. Sedlák, R., Kovalčíková, A., Balko, J., Rutkowski, P., Dubiel, A., Zientara, D., Girman, V., Múdra, E., Dusza, J.: Effect of graphene platelets on tribological properties of boron carbide ceramic composites. Int. J. Refract. Met. Hard Mater, 57–63 (2017)
32. Porwal, H., Tatarko, P., Saggar, R., Grasso, S., Kumar Mani, M., Dlouhý, I., Dusza, J., Reece, M.J.: Tribological properties of silica–graphene nano-platelet composites. Ceram. Int. **8, Part A**, 12067–12074 (2014)
33. Miranzo, P., García, E., Ramírez, C., González-Julián, J., Belmonte, M., Isabel Osendi, M.: Anisotropic thermal conductivity of silicon nitride ceramics containing carbon nanostructures. J. Eur. Ceram. Soc. **8**, 1847 (2012)
34. Balázsi, C., Fogarassy, Z., Tapasztó, O., Kailer, A., Schröder, C., Parchoviansky, M., Galusek, D., Dusza, J., Balázsi, K.: Si3N4/graphene nanocomposites for tribological application in aqueous environments prepared by attritor milling and hot pressing. J. Eur. Ceram. Soc. **12**, 3797–3804 (2017)
35. Llorente, J., Román-Manso, B., Miranzo, P., Belmonte, M.: Tribological performance under dry sliding conditions of graphene/silicon carbide composites. J. Eur. Ceram. Soc.
36. Llorente, J., Belmonte, M.: Friction and wear behaviour of silicon carbide/graphene composites under isooctane lubrication. Journal of the European Ceramic Society **10**, 3441–3446 (2018)
37. Maros B., M., Németh, A.K., Károly, Z., Bódis, E., Maros, Z., Tapasztó, O., Balázsi, K.: Tribological characterisation of silicon nitride/multilayer graphene nanocomposites produced by HIP and SPS technology. Tribol. Int., 269–281 (2016)

38. Hvizdoš, P., Dusza, J., Balázsi, C.: Tribological properties of Si3N4–graphene nanocomposites. J. Eur. Ceram. Soc. **12**, 2359–2364 (2013)
39. Beckert, F., Trenkle, S., Thomann, R., Mülhaupt, R.: Mechanochemical Route to Functionalized Graphene and Carbon Nanofillers for Graphene/SBR Nanocomposites. Macromol. Mater. Eng. **12**, 1513–1520 (2014)
40. Tschoppe, K., Beckert, F., Beckert, M., Mülhaupt, R.: Thermally Reduced Graphite Oxide and Mechanochemically Functionalized Graphene as Functional Fillers for Epoxy Nanocomposites. Macromol. Mater. Eng. **2**, 140–152 (2015)
41. Pereira dos Santos Tonello, K., Padovano, E., Badini, C., Biamino, S., Pavese, M., Fino, P.: Fabrication and characterization of laminated SiC composites reinforced with graphene nanoplatelets. Mater. Sci. Eng., A, 158–164 (2016)
42. Munro, R.G.: Material Properties of a Sintered α-SiC. Journal of Physical and Chemical Reference Data **5**, 1195–1203 (1997)